Acta Mechanica Solida Sinica, Vol. 28, No. 1, February, 2015
Published by AMSS Press, Wuhan, China
ISSN 0894-9166

VIBRATION AND SOUND RADIATION OF AN ASYMMETRIC LAMINATED PLATE IN THERMAL ENVIRONMENTS**

Wei Li **Yueming Li***

(*State Key Laboratory for Strength and Vibration of Mechanical Structures, Xi'an Jiaotong University, Xi'an* 710049, *China*)

Received 7 January 2013, revision received 22 January 2014

ABSTRACT Analytical studies on the vibration and sound radiation characteristics of an asymmetric laminated rectangular plate are carried out in this paper. Theoretical formulations, in which the effects of thermal environments are taken into account, are derived for the vibration and sound radiation based on both first-order shear deformation plate theory and Rayleigh integral. It is found that the natural frequencies, the resonant amplitudes of vibration response and the sound pressure level decrease with the temperature rising. The natural frequencies of asymmetric plates are smaller than those of symmetric plates and the velocity responses of asymmetric plates are larger than those of symmetric plates.

KEY WORDS asymmetric laminated plate, thermal environments, FSDPT, vibration, sound radiation

I. INTRODUCTION

Laminated plates are widely used in the field of aerospace, such as the aerocraft structures, which usually suffer serious aerodynamic heating in service. Thermal stresses caused by thermal environment change may induce buckling and influence dynamic characteristics.

A number of analytical and numerical solutions have been given for free vibration and buckling problems of composite laminates and sandwich plates. Reddy and Khdeir[1] studied the buckling and free vibration behavior of cross-ply rectangular composite laminates under different boundary conditions by analytical and finite element solutions of the classical, first-order, and third-order laminate theories. It is concluded that the shear deformation laminate theory is able to accurately predict the behavior of composite laminates, whereas the classical laminate theory over-predicts natural frequencies and buckling loads. In Ref.[2], exact solutions were presented for the free vibration of symmetrically laminated composite beams with first-order shear deformation and rotary inertia considered in analysis. Asghar et al.[3] used Reddy's layer-wise theory to conduct free vibration analysis of laminated plates. Kant and Swaminathan[4] analyzed the free vibration of composite laminates and sandwich plates based on a higher-order refined theory, which accounted for the effects of transverse shear deformation, transverse normal strain/stress and nonlinear variation of in-plane displacements with respect to the thickness coordinate. Ganapathi and Makhecha[5] presented an accurate higher-order theory using the finite element procedure for the free vibration analysis of multi-layered thick composite plates. Liew

* Corresponding author. E-mail: liyueming@mail.xjtu.edu.cn
** Project supported by the National Natural Science Foundation of China (Nos. 11321062, 91016008 and 91216107).

et al.[6] adopted the first-order shear deformation theory for predicting the free vibration behavior of moderately thick symmetrically laminated composite plates. Shooshtari and Razavi[7] gave a closed form answer analytically to linear and nonlinear free vibrations of composites based on the first-order shear deformation theory.

With respect to the influence of the temperature, Fauconneau and Marangoni[8] investigated the effect of a constant thermal gradient on the transverse vibrational frequencies of a simply supported rectangular plate. Prabhu and Dhanaraj[9] analyzed the thermal buckling of laminated composite plates using FEM based on the first-order shear deformation theory. Free and forced vibration analyses for initially stressed functionally graded plates in a thermal environment were presented in Ref.[10]. Matsunaga[11] presented a two-dimensional global higher-order deformation theory for the free vibration and stability problems of angle-ply laminated composites subjected to thermal loading. Pradeep and Ganesan[12] studied the free vibration and damping characteristics of plates consisting of composite stiff-layers and an isotropic viscoelastic core under thermal loads using FEM. A decoupled thermo-mechanical analysis was made using the finite element method[13]. In the study, a four-side clamped plate with constant temperature throughout the plate domain was analyzed for thermal buckling, frequency and damping behavior, and the variation trends of these characteristics against temperature were indicated as well. Jeyaraj et al.[14] presented numerical studies on the vibration and acoustic response characteristics of a composite plate in a thermal environment considering the inherent material damping property of the composite material based on the classical laminated plate theory and coupled FEM/BEM technique. The influence of thermal environments on the dynamic response and acoustic characteristics were investigated in Ref.[15], in which theoretical expressions were derived first for the vibration and acoustic radiation of a simply supported rectangular thin plate by considering the membrane forces induced by thermal environment change. It is reported in Refs.[16] and [17] that structural topology optimization has been carried out to minimize the radiated acoustic power and structural dynamic compliance in a thermal environment .

In the present work, the analytical vibration solution of an asymmetric laminated plate in a thermal environment is solved by employing the first-order shear deformation plate theory (FSDPT), in which shear deformation and rotary inertia are involved, and then the sound radiation characteristics of the laminated plates are obtained using Rayleigh integral analytically. The variation of natural frequencies and sound radiation characteristics with temperature has been studied. Validation studies are also done and a good agreement with numerical solutions calculated by commercial software is achieved.

II. FORMULATIONS

The displacement fields based on the FSDPT of the laminated plate (Fig.1) are given by

$$\begin{aligned} u(x,y,z,t) &= u^0(x,y,t) + z\varphi_x(x,y,t) \\ v(x,y,z,t) &= v^0(x,y,t) + z\varphi_y(x,y,t) \\ w(x,y,z,t) &= w(x,y,t) \end{aligned} \tag{1}$$

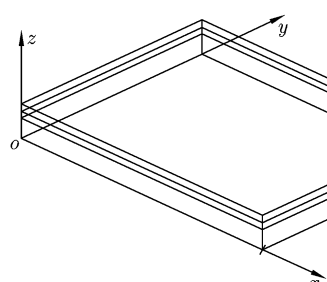

Fig. 1. Laminated plate.

where u, v and w are the displacements along x, y and z directions with x and y on the plane of the plate and z along the thickness direction, and φ_x, φ_y are the rotations of a transverse normal about the y- and x-axes. All of the letters with ^{0} stand for the value of mid-surface.

Since the material and thickness of the laminated plate are asymmetric in the present study, bending-extensional coupling matrix [B] will result. So the derivation with the present approach is more difficult and complicated than that with the Classical Laminated Plates Theory.

The strain displacement relations are

$$\begin{aligned}&\varepsilon_x=\frac{\partial u^0}{\partial x}+z\frac{\partial\varphi_x}{\partial x},\quad \varepsilon_y=\frac{\partial v^0}{\partial y}+z\frac{\partial\varphi_y}{\partial y},\quad \gamma_{xy}=\frac{\partial u^0}{\partial y}+\frac{\partial v^0}{\partial x}+z(\frac{\partial\varphi_x}{\partial y}+\frac{\partial\varphi_y}{\partial x})\\&\gamma_{yz}=\gamma_{yz}^0=\frac{\partial w}{\partial y}+\varphi_y,\quad \gamma_{xz}=\gamma_{xz}^0=\frac{\partial w}{\partial x}+\varphi_x,\quad \varepsilon_z=0\end{aligned}\tag{2}$$

$$\begin{aligned}&\varepsilon_x^0=\frac{\partial u^0}{\partial x},\quad \chi_x=\frac{\partial\varphi_x}{\partial x},\quad \varepsilon_y^0=\frac{\partial v^0}{\partial y},\quad \chi_y=\frac{\partial\varphi_y}{\partial y}\\&\gamma_{xy}^0=\frac{\partial u^0}{\partial y}+\frac{\partial v^0}{\partial x},\quad \chi_{xy}=\frac{\partial\varphi_x}{\partial y}+\frac{\partial\varphi_y}{\partial x}\end{aligned}\tag{3}$$

The stress and moment resultants of a laminated plate made up of N layers of orthotropic plates and subjected to a uniform temperature rise of ΔT can be expressed as follows:

$$\begin{Bmatrix}\{N\}\\\{M\}\end{Bmatrix}=\begin{bmatrix}[A]&[B]^{\mathrm T}\\{}[B]&[D]\end{bmatrix}\begin{Bmatrix}\{\varepsilon^0\}\\\{\chi\}\end{Bmatrix}-\begin{Bmatrix}\{\overline{N}\}\\\{\overline{M}\}\end{Bmatrix}\tag{4}$$

where

$$\begin{Bmatrix}\overline{N}_x&\overline{M}_x\\\overline{N}_y&\overline{M}_y\\\overline{N}_{xy}&\overline{M}_{xy}\end{Bmatrix}=\sum_{k=1}^{n}\int_{z_{k-1}}^{z_k}\begin{bmatrix}C_{11}&C_{12}&0\\C_{21}&C_{22}&0\\0&0&C_{66}\end{bmatrix}\begin{Bmatrix}\alpha_x\\\alpha_y\\\alpha_{xy}\end{Bmatrix}_k\Delta T_k\{1\quad z\}\mathrm{d}z$$

and α_x, α_y, α_{xy} are the coefficients of thermal expansion along x, y and shear directions,

$$\begin{aligned}&\{N\}=\{\,N_x\quad N_y\quad N_{xy}\,\}^{\mathrm T},\quad \{M\}=\{\,M_x\quad M_y\quad M_{xy}\,\}^{\mathrm T}\\&\{\varepsilon^0\}=\{\,\varepsilon_x^0\quad \varepsilon_y^0\quad \gamma_{xy}^0\,\}^{\mathrm T},\quad \{\chi\}=\{\,\chi_x\quad \chi_y\quad \chi_{xy}\,\}^{\mathrm T}\end{aligned}$$

A_{ij}, B_{ij} and D_{ij} are the coefficients of extensional, bending-extensional coupling, and bending stiffness matrices. Bending-extensional coupling matrix [B] is caused by asymmetry. These are obtained as

$$[A]=\int[C]\mathrm{d}z,\quad [B]=\int z\cdot[C]\mathrm{d}z,\quad [D]=\int z^2\cdot[C]\mathrm{d}z$$

where $[C]$ is the stiffness matrix.

In the FSDPT, Q_x and Q_y are considered, which are called the transverse shear stress. The transverse shear stress resultants are given as

$$\begin{Bmatrix}Q_x\\Q_y\end{Bmatrix}=\kappa\begin{bmatrix}A_{44}&0\\0&A_{55}\end{bmatrix}\begin{Bmatrix}\gamma_{xz}^0\\\gamma_{yz}^0\end{Bmatrix}\tag{5}$$

where κ is the shear correction coefficient. The usual value of κ is 1, 5/6, $\sqrt{3}/2$. The governing equations of the FSDPT will be derived using Hamilton's principle:

$$\int\delta(U+V-T)\mathrm{d}t=0\tag{6}$$

where δU is the virtual strain energy, δV is the virtual potential energy caused by thermal stress and external force, and δT is the virtual kinetic energy.

By performing Hamilton's principle, five equations of motion are obtained as

$$\begin{aligned}&N_{x,x}+N_{xy,y}=R_0u^0_{,tt}+R_1\varphi_{x,tt}\\&N_{xy,x}+N_{y,y}=R_0v^0_{,tt}+R_1\varphi_{y,tt}\\&Q_{x,x}+Q_{y,y}+\overline{N}_x\frac{\partial^2w}{\partial x^2}++\overline{N}_y\frac{\partial^2w}{\partial y^2}+2\overline{N}_{xy}\frac{\partial^2w}{\partial x\partial y}+q=R_0w_{,tt}\\&M_{x,x}+M_{xy,y}-Q_x=R_1u^0_{,tt}+R_2\varphi_{x,tt}\\&M_{xy,x}+M_{y,y}-Q_y=R_1v^0_{,tt}+R_2\varphi_{y,tt}\end{aligned}\tag{7}$$

where

$$R_0=\int\rho \mathrm{d}z,\quad R_1=\int\rho z\mathrm{d}z,\quad R_2=\int\rho z^2\mathrm{d}z$$

The thermal influence is reflected in the third equation in Eq.(7).

By substituting Eq.(3) into Eq.(4) and substituting the answer to the last step into Eq.(7), the governing equations in terms of displacements are obtained as

$$\begin{aligned}
&A_{11}\frac{\partial^2u^0}{\partial x^2}+A_{12}\frac{\partial^2v^0}{\partial x\partial y}+B_{11}\frac{\partial^2\varphi_x}{\partial x^2}+B_{12}\frac{\partial^2\varphi_y}{\partial x\partial y}+A_{66}\frac{\partial^2u^0}{\partial y^2}+A_{66}\frac{\partial^2v^0}{\partial y\partial x}+B_{66}\frac{\partial^2\varphi_x}{\partial y^2}+B_{66}\frac{\partial^2\varphi_y}{\partial x\partial y}\\
&\quad=R_0\frac{\partial^2u^0}{\partial t^2}+R_1\frac{\partial^2\varphi_x}{\partial t^2}\\
&A_{66}\frac{\partial^2u^0}{\partial x\partial y}+A_{66}\frac{\partial^2v^0}{\partial x^2}+B_{66}\frac{\partial^2\varphi_x}{\partial x\partial y}+B_{66}\frac{\partial^2\varphi_y}{\partial x^2}+A_{21}\frac{\partial^2u^0}{\partial x\partial y}+A_{22}\frac{\partial^2v^0}{\partial y^2}+B_{21}\frac{\partial^2\varphi_x}{\partial x\partial y}+B_{22}\frac{\partial^2\varphi_y}{\partial y^2}\\
&\quad=R_0\frac{\partial^2v^0}{\partial t^2}+R_1\frac{\partial^2\varphi_y}{\partial t^2}\\
&\kappa(A_{55}\frac{\partial^2w}{\partial x^2}+A_{55}\frac{\partial\varphi_x}{\partial x}+A_{44}\frac{\partial^2w}{\partial y^2}+A_{44}\frac{\partial\varphi_y}{\partial y})+\overline{N}_x\frac{\partial^2w}{\partial x^2}+\overline{N}_y\frac{\partial^2w}{\partial y^2}+q=R_0\frac{\partial^2w}{\partial t^2}\\
&B_{11}\frac{\partial^2u^0}{\partial x^2}+B_{12}\frac{\partial^2v^0}{\partial x\partial y}+D_{11}\frac{\partial^2\varphi_x}{\partial x^2}+D_{12}\frac{\partial^2\varphi_y}{\partial x\partial y}+B_{66}\frac{\partial^2u^0}{\partial y^2}+B_{66}\frac{\partial^2v^0}{\partial y\partial x}\\
&\qquad+D_{66}\frac{\partial^2\varphi_x}{\partial y^2}+D_{66}\frac{\partial^2\varphi_y}{\partial x\partial y}-\kappa A_{55}(\frac{\partial w}{\partial x}+\varphi_x)=R_1\frac{\partial^2u^0}{\partial t^2}+R_2\frac{\partial^2\varphi_x}{\partial t^2}\\
&B_{66}\frac{\partial^2u^0}{\partial x\partial y}+B_{66}\frac{\partial^2v^0}{\partial x^2}+D_{66}\frac{\partial^2\varphi_x}{\partial x\partial y}+D_{66}\frac{\partial^2\varphi_y}{\partial x^2}+B_{21}\frac{\partial^2u^0}{\partial x\partial y}+B_{22}\frac{\partial^2v^0}{\partial y^2}\\
&\qquad+D_{21}\frac{\partial^2\varphi_x}{\partial x\partial y}+D_{22}\frac{\partial^2\varphi_y}{\partial y^2}-\kappa A_{44}(\frac{\partial w}{\partial y}+\varphi_y)=R_1\frac{\partial^2v^0}{\partial t^2}+R_2\frac{\partial^2\varphi_y}{\partial t^2}
\end{aligned}\tag{8}$$

For free vibration ($q=0$), the displacements can be written in the form of

$$\begin{aligned}
u^0(x,y,t)&=U_{mn}(x,y)\sin(\omega_{mn}t+\phi_0)\\
v^0(x,y,t)&=V_{mn}(x,y)\sin(\omega_{mn}t+\phi_0)\\
w(x,y,t)&=W_{mn}(x,y)\sin(\omega_{mn}t+\phi_0)\\
\varphi_x(x,y,t)&=\varphi^x_{mn}(x,y)\sin(\omega_{mn}t+\phi_0)\\
\varphi_y(x,y,t)&=\varphi^y_{mn}(x,y)\sin(\omega_{mn}t+\phi_0)
\end{aligned}\tag{9}$$

where ω_{mn} is the natural frequency.

Orthogonality of laminate is obtained based on Hamilton's principle:

$$\begin{aligned}
&\int\!\!\int[(U_{mn}U_{kl}+V_{mn}V_{kl}+W_{mn}W_{kl})R_0+(U_{mn}\varphi^x_{kl}+U_{kl}\varphi^x_{mn}+V_{mn}\varphi^y_{kl}+V_{kl}\varphi^y_{mn})R_1\\
&\qquad+(\varphi^x_{mn}\varphi^x_{kl}+\varphi^y_{mn}\varphi^y_{kl})R_2]\,\mathrm{d}x\mathrm{d}y\begin{cases}=0 & (m\neq k,\ n\neq l)\\ \neq 0 & (m=k,\ n=l)\end{cases}
\end{aligned}\tag{10}$$

M is defined as the general mass.

$$\begin{aligned}
M=&\int\!\!\int[(U^2_{mn}+V^2_{mn}+W^2_{mn})R_0+(U_{mn}\varphi^x_{mn}+U_{mn}\varphi^x_{mn}+V_{mn}\varphi^y_{mn}+V_{mn}\varphi^y_{mn})R_1\\
&+(\varphi^x_{mn}\varphi^x_{mn}+\varphi^y_{mn}\varphi^y_{mn})R_2]\,\mathrm{d}x\mathrm{d}y
\end{aligned}$$

By considering a simply supported laminated rectangular plate with orthotropic layers, the vibration functions can be written in the form of

$$\begin{aligned}
U_{mn}&=\overline{A}_{mn}\cos\left(\frac{m\pi x}{a}\right)\sin\left(\frac{n\pi y}{b}\right)\\
V_{mn}&=\overline{B}_{mn}\sin\left(\frac{m\pi x}{a}\right)\cos\left(\frac{n\pi y}{b}\right)\\
W_{mn}&=\overline{C}_{mn}\sin\left(\frac{m\pi x}{a}\right)\sin\left(\frac{n\pi y}{b}\right)\\
\varphi^x_{mn}&=\overline{D}_{mn}\cos\left(\frac{m\pi x}{a}\right)\sin\left(\frac{n\pi y}{b}\right)\\
\varphi^y_{mn}&=\overline{E}_{mn}\sin\left(\frac{m\pi x}{a}\right)\cos\left(\frac{n\pi y}{b}\right)
\end{aligned}\tag{11}$$

where a and b are length and width, respectively.

By considering Eq.(8), Eq.(9) and Eq.(11), the homogeneous linearly algebraic equations are obtained as written below:

$$[H]\left\{\overline{A}_{mn}\ \overline{B}_{mn}\ \overline{C}_{mn}\ \overline{D}_{mn}\ \overline{E}_{mn}\right\}^{\mathrm{T}}=0 \tag{12}$$

The natural frequency ω can be solved by setting $\det([H])=0$, and the critical temperature T_{cr} can be determined by setting $\det([H])=0$ with $\omega_{11}=0$

Substitute ω_{mn} into Eq.(12) and $M=1$, $\overline{A}_{mn}$, $\overline{B}_{mn}$, $\overline{C}_{mn}$, $\overline{D}_{mn}$ and $\overline{E}_{mn}$ are obtained. So the vibration shape functions are solved.

For the forced vibration under harmonic excitation, the transverse vibration displacement can be written in the form of

$$w(x,y,t)=\sum_{m}\sum_{n}W_{mn}(x,y)T_{mn}(t) \tag{13}$$

Considering Eq.(8) and Eq.(10), we have the equation for $T_{mn}(t)$:

$$\ddot{T}_{mn}(t)+\omega_{mn}^{2}T_{mn}(t)=Q_{mn} \tag{14}$$

where $Q_{mn}=\int\int q{\cdot}W_{mn}\mathrm{e}^{\mathrm{j}\omega t}\mathrm{d}x\mathrm{d}y$.

The solution of Eq.(13) is obtained as

$$w(x,y,t)=\sum_{m}\sum_{n}W_{mn}(x,y)\frac{Q_{mn}}{\omega_{mn}^{2}-\omega^{2}}\mathrm{e}^{\mathrm{j}\omega t} \tag{15}$$

According to Rayleigh integral, the sound pressure radiated from a vibrating plate is

$$p\left(x_p,y_p,z_p,t\right)=\frac{\mathrm{j}\omega\rho_0}{2\pi}\mathrm{e}^{\mathrm{j}\omega t}\int_{\Omega}\frac{\widetilde{v}(x,y,t)\cdot\mathrm{e}^{-\mathrm{j}kR}}{R}\mathrm{d}A \tag{16}$$

where ρ_0 is air density, $R=\sqrt{(x_p-x)^2+(y_p-y)^2+(z_p-z)^2}$ is the distance between the observation point (x_p,y_p,z_p) in the acoustic field and the integration point, k is given by the excitation frequency and sound speed as $k=\omega/c_0$, $\widetilde{v}(x,y,t)$ is the first derivative of $w(x,y,t)$.

III. VALIDATION STUDIES

Case 1: A validation is conducted between the present method and Liu's work[18]. The parameters and material properties of the sandwich plate calculated are also taken from Ref.[18].

Case 2: A simply supported laminated rectangular plate with dimensions of 0.3 m $\times$ 0.4 m is considered for the validation and comparison of the present method and commercial software. The material properties and thickness are given in Table 1. The ambient temperature is 0 °C and the shear corrector κ is 1.

Table 1. **Material properties and parameters of laminated plate**

	Density(kg/m^3)	Young's modulus(GPa)	Poisson's ratio	Thermal expansion(/K)	Thickness(m)
Ti	4500	110(1+0.01j)	0.33	1×10^{-5}	2×10^{-3}
Al	2700	70(1+0.01j)	0.3	2.3×10^{-5}	5×10^{-3}
Steel	7850	200(1+0.01j)	0.27	8×10^{-6}	3×10^{-3}

3.1. Validation for Critical Buckling Temperature Evaluation

Taking $m=1$ and $n=1$, we can get the first mode of the plate in case 2.

The critical temperature T_{cr} is 99 °C obtained by the Eq.(12) in case 2. It matches well the value, which is 102 °C, obtained by FEM(Nastran).

Table 2. **Comparison of natural frequency (Hz) with that obtained by Liu**

Sequence	Mode	$\Delta T = 0\,^\circ$C		$\Delta T = 50\,^\circ$C	
		Present	Liu's	Present	Liu's
1	(1,1)	372.86	371.26	257.76	255.44
2	(2,1)	772.28	765.49	667.63	659.75
3	(1,2)	1080.65	1067.5	978.04	963.44
4	(3,1)	1430.67	1407.8	1329.11	1304.5
5	(2,2)	1474.24	1450	1372.77	1346.7

Table 3. **Comparison of natural frequency (Hz) with that obtained with FEM (Nastran)**

Sequence	Mode	$\Delta T = 0\,^\circ$C			$\Delta T = 60\,^\circ$C		
		Present	FEM (Nastran)	Error (%)	Present	FEM (Nastran)	Error (%)
1	(1,1)	449.41	450	0.13	289	283.23	−2.03
2	(2,1)	931.63	919	−1.37	772	784.31	1.57
3	(1,2)	1304.98	1290	−1.16	1140	1161.28	1.83
4	(3,1)	1728.58	1700	−1.68	1560	1586.76	1.69
5	(2,2)	1780.69	1750	−1.75	1610	1638.97	1.77

3.2. Validation for Natural Frequencies

Case 1: The natural frequencies are obtained by the present approach with $\Delta T = 0\,^\circ$C and $\Delta T = 50\,^\circ$C. Table 2 shows the results in good agreement with Liu's.

Case 2: The natural frequencies obtained by the present approach and FEM(Nastran) with $\Delta T = 0\,^\circ$C and $\Delta T = 60\,^\circ$C are illustrated in Table 3, which shows a good agreement with small errors in both conditions. So the present approach to calculating natural frequency is applicable.

3.3. Validation for Forced Vibration and Sound Radiation Calculation

A harmonic point excitation of 1 N is applied to the plate in both cases. Given the damping ratio 0.01 for all modes in harmonic response analysis, it is assumed that the plate is vibrating in air of density $\rho_k = 1.21$ kg/m^3 with a speed of sound $c = 343$ m/s. The velocity response is calculated according to the forced vibration analysis and the sound pressure level of the plate is calculated using Rayleigh integral.

Case 1: The excitation is applied at the point (0.1, 0.1, 0). The velocity response and sound pressure response are calculated with $\Delta T = 0\,^\circ$C and $\Delta T = 50\,^\circ$C. The velocity obtained using the present approach is compared with the results of Liu's, as shown in Figs.2 and 3, and the comparison of sound pressure level is shown in Figs.4 and 5. It is obvious from these curves that there is a good agreement between the results of the present approach and Liu's. So the present approach to forced vibration and sound radiation calculation is applicable.

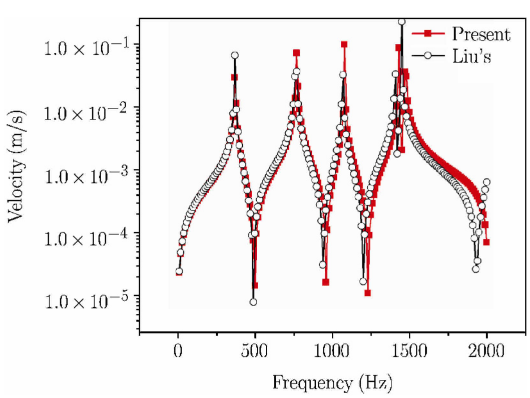

Fig. 2. Comparison of velocity with Liu's results ($\Delta T = 0\,^\circ$C).

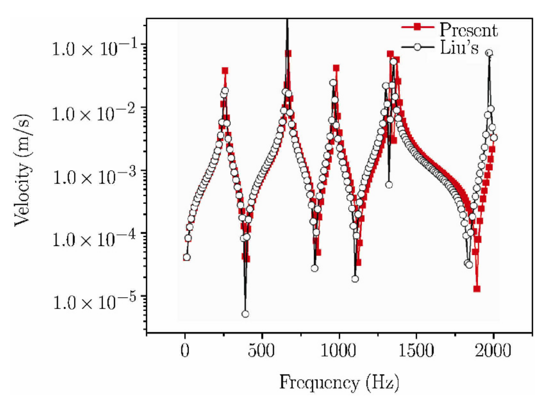

Fig. 3. Comparison of velocity with Liu's results ($\Delta T = 50\,^\circ$C).

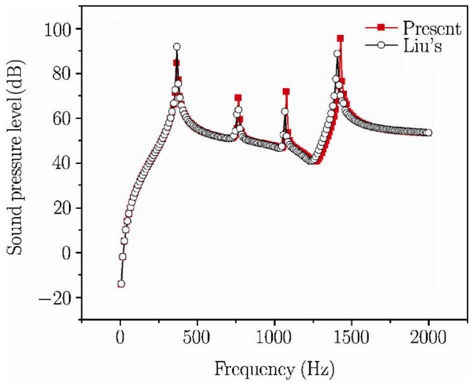

Fig. 4. Comparison of sound pressure level with Liu's results ($\Delta T = 0\,^\circ$C).

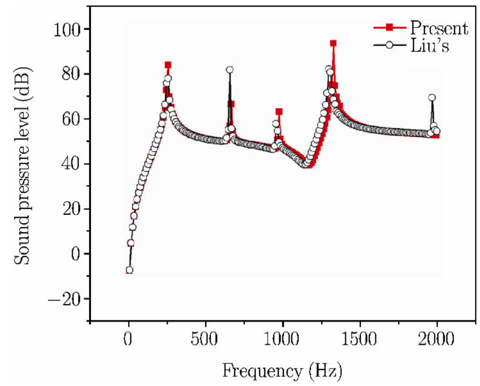

Fig. 5. Comparison of sound pressure level with Liu's results ($\Delta T = 50\,^\circ$C).

Case 2: The excitation is applied at a quarter of the plate. The observation point of velocity is $(0.25 \times a,\ 0.25 \times b,\ 0)$ and the observation point of sound pressure level is $(0.25 \times a,\ 0.25 \times b,\ 3)$.

In this study, calculation is conducted with $\Delta T = 0\,^\circ$C and $\Delta T = 60\,^\circ$C. A numerical model for validating is built in commercial software VA One, as shown in Fig.6.

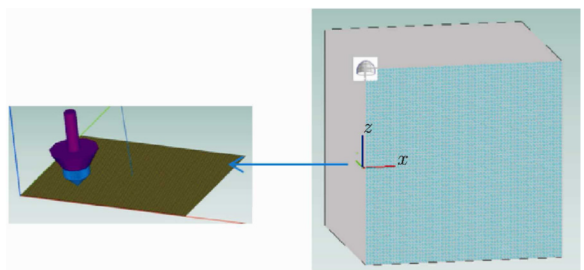

Fig. 6. FEM and BEM models in VA One.

The comparison of velocity obtained using the present approach with the results calculated by VA One is shown in Figs.7 and 8. The sound pressure level obtained using the present approach is compared with the results calculated by commercial software VA One shown in Figs.9 and 10. It is obvious that there is a good agreement between the results of the present approach and VA One. So the present approach to forced vibration and sound radiation calculation is applicable.

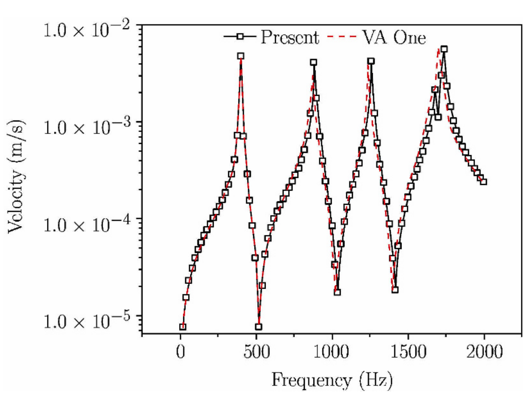

Fig. 7. Comparison of velocity with $\Delta T = 0\,^\circ$C.

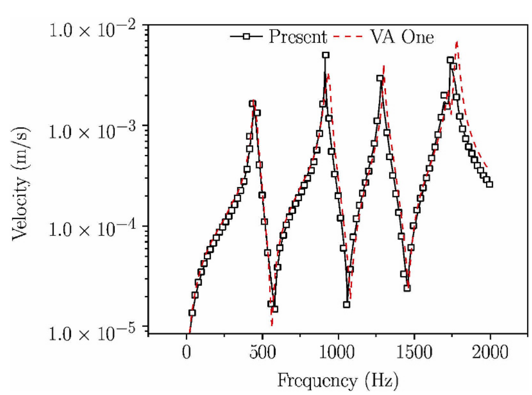

Fig. 8. Comparison of velocity with $\Delta T = 60\,^\circ$C.

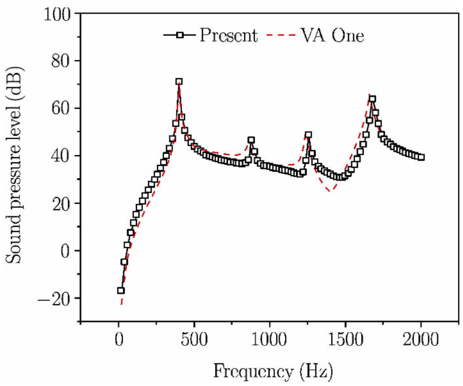

Fig. 9. Comparison of sound pressure level with the numerical results ($\Delta T = 0\,^{\circ}$C).

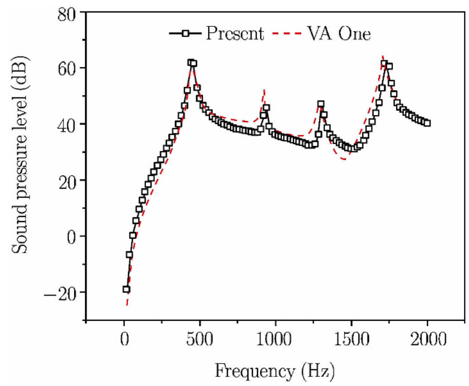

Fig. 10. Comparison of sound pressure level with the numerical results ($\Delta T = 60\,^{\circ}$C).

IV. VARIOUS RESULTS AND DISCUSSION

Choose the plate in case 2 as the object for these studies, keeping all of the excitation and ambient conditions unchanged. The uniform temperature rise applied on the plate varies from $\Delta T = 0\,^{\circ}$C to $\Delta T = 90\,^{\circ}$ in steps of 30 °C. The corresponding natural frequency variation, vibration and acoustic responses have been analyzed in order to investigate the influence of the thermal environment on the dynamic and acoustic responses.

4.1. Vibration Studies

In order to compare the vibration response, the displacement and velocity response to the point of excitation, calculations are made at different levels of rise of uniform temperature ΔT within the 20-2000 Hz frequency range for analysis.

Table 4 gives the natural frequencies and mode shapes, and Fig.11 shows the variation in natural frequencies at different ΔTs. It is seen that the natural frequencies decrease with an increase in temperature, while the mode shapes remain the same.

Table 4. **Natural frequencies and mode shapes at different uniform temperature rise**

Sequence	$\Delta T = 0\,^{\circ}$C		$\Delta T = 30\,^{\circ}$C	
	Mode shapes	Frequency (Hz)	Mode shapes	Frequency (Hz)
1	(1,1)	449.42	(1,1)	375.63
2	(2,1)	931.64	(2,1)	861.13
3	(1,2)	1304.99	(1,2)	1235.23
4	(3,1)	1728.60	(3,1)	1659.20
5	(2,2)	1780.71	(2,2)	1711.31
Sequence	$\Delta T = 60\,^{\circ}$C		$\Delta T = 90\,^{\circ}$C	
	Mode shapes	Frequency (Hz)	Mode shapes	Frequency (Hz)
1	(1,1)	283.23	(1,1)	139.20
2	(2,1)	784.31	(2,1)	699.10
3	(1,2)	1161.28	(1,2)	1082.29
4	(3,1)	1586.76	(3,1)	1510.85
5	(2,2)	1638.97	(2,2)	1563.29

The thermal stress will reduce the stiffness of the structure, and the softening effect will reduce the natural frequency. The influence on the fundamental frequency is most obvious.

The displacement response, velocity response, and mean square velocity are shown in Figs.12-14, respectively. It can be found that the resonant frequencies decrease with an increase in ΔT. Although the variation in resonant amplitudes of the displacement response is not obvious, the resonant amplitudes of the velocity and the mean square velocity decrease obviously with an increase in ΔT. The velocity is calculated by multiplying displacement by the corresponding forced frequency. When the variation in

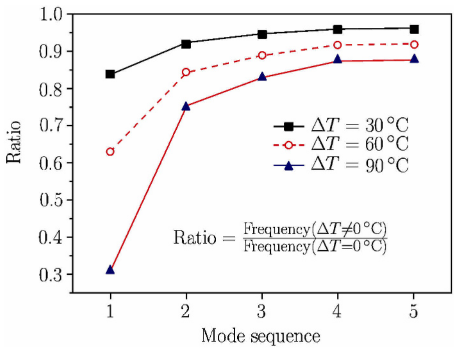

Fig. 11. Variations of natural frequencies at different uniform temperature rise.

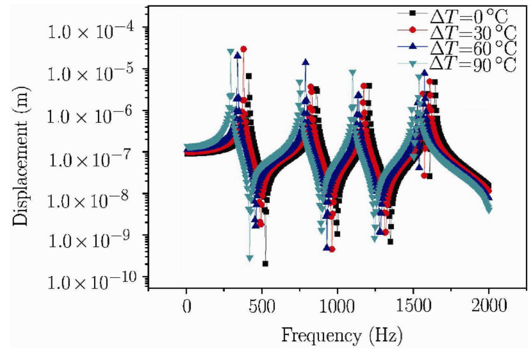

Fig. 12. Displacement of the excitation point at different uniform temperature rise.

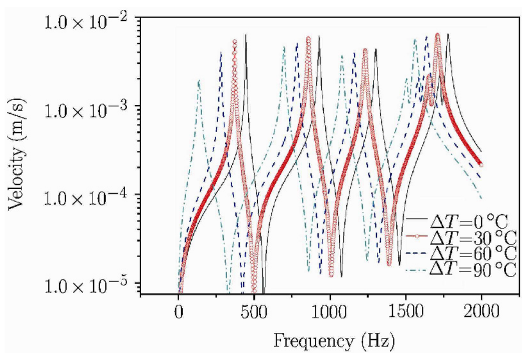

Fig. 13. Velocity of the excitation point at different uniform temperature rise.

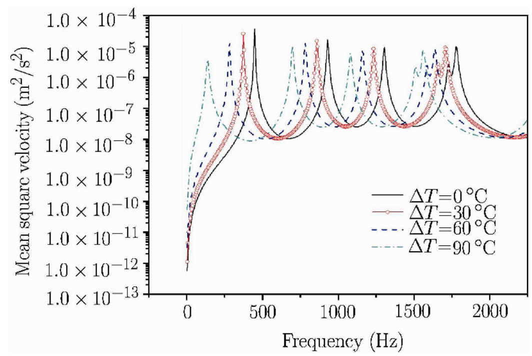

Fig. 14. Mean square velocity of the vibrating plate at different uniform temperature rise.

resonant amplitudes of the displacement response is small and the resonant frequencies decrease with increasing ΔT, the resonant amplitudes of the velocity and the mean square velocity will be reduced.

4.2. Sound Radiation Studies

The sound pressure level, sound power and sound radiation efficiency are also calculated for different ΔTs. Figures 15 and 16 show the sound pressure level and output sound power, respectively. The two characteristics have the same trends as the velocity response as they are influenced by the vibration velocity directly. And the resonant frequency tends to narrow the frequency range.

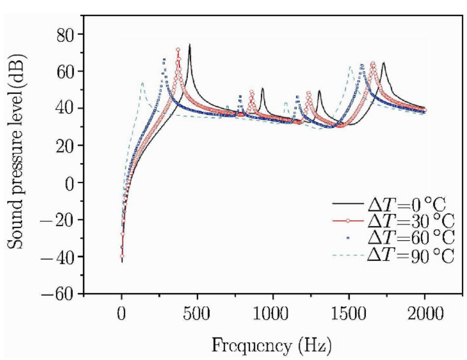

Fig. 15. Sound pressure level of the observation point in acoustic field at different uniform temperature rise.

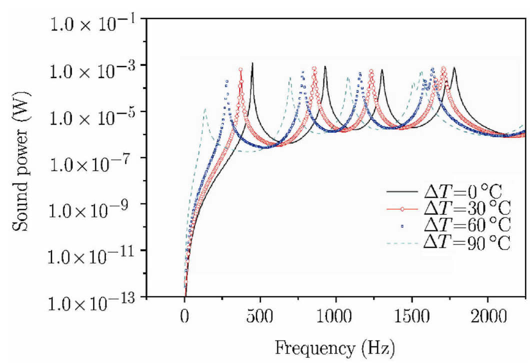

Fig. 16. Sound radiation power of the vibrating plate at different uniform temperature rise.

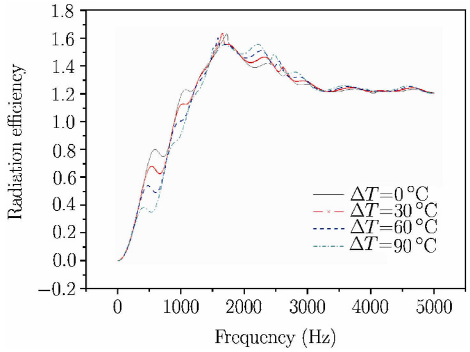

Fig. 17. Radiation efficiency of the vibrating plate at different values of uniform temperature rise.

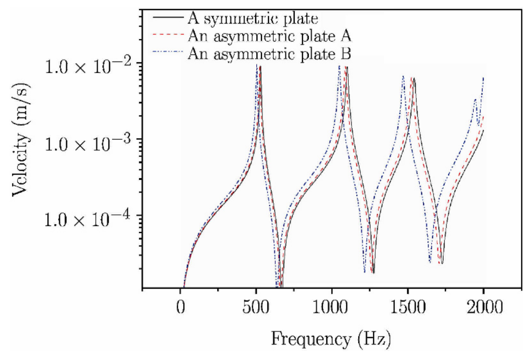

Fig. 18. Comparison of velocity responses.

Figure 17 shows the radiation efficiency of the vibrating plate in different thermal environments. It can be found that radiation efficiency decreases with the increase of ΔT when the frequency below 2000 Hz. The radiation efficiency, however, turns to increase with ΔT and towards a flat line when the frequency is in a range of 2000-5000 Hz.

4.3. Comparison between Asymmetric Plates and a Symmetric Plate

A comparison between two asymmetric plates and a symmetric plate is conducted. Table 5 lists the material properties and thicknesses. The free vibration and forced vibration are calculated for the three plates by the present approach. The coefficients of extensional, bending-extensional coupling and bending stiffness matrices are obtained as shown in Table 6. As listed, the coefficients of bending extensional coupling stiffness matrixes of asymmetric plates are larger and those of bending stiffness matrixes are smaller compared with the symmetric plate. For the bending stiffness decreasing with an increase in asymmetry, the natural frequencies of asymmetric plates are smaller than those of the symmetric plate and the velocity responses of asymmetric plates are larger than those of the symmetric plate, as shown in Table 7 and Fig.18.

Table 5. **Materials properties**

	Density (kg/m^3)	Young's modulus (GPa)	Poisson's ratio	Thermal expansion	Thickness (m)
	2700	110(1+0.01j)	0.33	1.00×10^{-5}	0.003
Symmetric plate	2700	70(1+0.01j)	0.3	2.30×10^{-5}	0.004
	2700	110(1+0.01j)	0.33	1.00×10^{-5}	0.003
	2700	110(1+0.01j)	0.33	1.00×10^{-5}	0.002
Asymmetric plate A	2700	70(1+0.01j)	0.3	2.30×10^{-5}	0.004
	2700	110(1+0.01j)	0.33	1.00×10^{-5}	0.004
	2700	110(1+0.01j)	0.33	1.00×10^{-5}	0.001
Asymmetric plate B	2700	70(1+0.01j)	0.3	2.30×10^{-5}	0.004
	2700	110(1+0.01j)	0.33	1.00×10^{-5}	0.005

Table 6. **Coefficients of extensional, bending-extensional coupling, and bending stiffness matrixes**

	A_{11}	A_{12}	A_{44}	B_{11}	B_{12}	B_{66}
Symmetric plate	1.07×10^9	3.75×10^9	3.49×10^9	0	0	0
Asymmetric plate A	1.07×10^9	3.75×10^9	3.49×10^9	2.02×10^5	9.63×10^4	5.29×10^9
Asymmetric plate B	1.07×10^9	3.75×10^9	3.49×10^9	4.04×10^5	1.93×10^5	1.06×10^5
	D_{11}	D_{12}	D_{66}	R_0	R_1	R_2
Symmetric plate	1.04×10^4	3.80×10^3	3.28×10^3	27	0	2.25×10^{-4}
Asymmetric plate A	1.01×10^4	3.70×10^3	3.22×10^3	27	0	2.25×10^{-4}
Asymmetric plate B	9.54×10^3	3.42×10^3	3.06×10^3	27	0	2.25×10^{-4}

Table 7. **Natural frequencies**

Sequence	Mode	A symmetric plate	An asymmetric plate A	An asymmetric plate B
1	(1,1)	532.24	526.06	507.05
2	(2,1)	1103.22	1090.47	1051.26
3	(1,2)	1544.61	1526.83	1472.12
4	(3,1)	2046.20	2022.75	1950.58
5	(2,2)	2108.69	2084.53	2010.19

V. CONCLUSIONS

The effects of thermal environments on the vibration and sound radiation characteristics of an asymmetric laminated plate are discussed in the present work. Theoretical formulations with the effects of thermal environments taken into account are derived for the vibration and the sound radiation based on the first-order shear deformation theory and Rayleigh integral.

Numerical simulations with Nastran and VA One are used to validate the theoretical results that agree well with the numerical ones.

The natural frequencies, deformation response and velocity response at the excitation point, the mean square velocity, sound pressure level and output sound power are calculated for different values of uniform temperature rise below the critical temperature with the present approach. The comparison between asymmetric plates and the symmetric plate is conducted.

It is found that the natural frequencies decrease with the uniform temperature rise, and the resonant amplitudes of vibration response and the sound pressure level response are reduced with the increase in temperature. The natural frequencies of asymmetric plates are smaller than those of the symmetric plate, while the velocity responses of asymmetric plates are larger than those of the symmetric plate.

References

[1] Reddy,J.N. and Khdeir,A.A., Buckling and vibration of laminated composite plates using various plate theories. *AIAA Journal*, 1989, 27(12): 1808-1817.

[2] Chandrashekhara,K., Krishnamurthy,K. and Roy,S., Free vibration of composite beams including rotary inertia and shear deformation. *Composite Structures*, 1990, 14: 269-279.

[3] Asghar,N., Kapania,R.K. and Reddy,J.N., Free vibration analysis of laminated plates using a layer-wise theory. *AIAA Journal*, 1993, 31: 2335-2346.

[4] Kant,T. and Swaminathan,K., Analytical solutions for free vibration of laminated composite and sandwich plates based on a higher-order refined theory. *Composite Structures*, 2001, 53: 73-85.

[5] Ganapathi,M. and Makhecha,D.P., Free vibration analysis of multi-layered composite laminates based on an accurate higher-order theory. *Composites Part B: Engineering*, 2001, 32: 535-543.

[6] Liew,K.M., Huang,Y.Q. and Reddy,J.N., Vibration analysis of symmetrically laminated plates based on FSDT using the moving least squares differential quadrature method. *Computer Methods in Applied Mechanics and Engineering*, 2003, 192: 2203-2222.

[7] Shooshtari,A. and Razavi,S., A closed form solution for linear and nonlinear free vibrations of composite and fiber metal laminated rectangular plates. *Composite Structures*, 2010, 92: 2663-2675.

[8] Fauconneau,G. and Marangoni,R.D., Effect of a thermal gradient on the natural frequencies of a rectangular plate. *International Journal of Mechanical Sciences*, 1970, 12: 113-122.

[9] Prabhu,M.R. and Dhanaraj,R., Thermal buckling of laminated composite plates. *Computers & amp; Structures*, 1994, 53: 1193-1204.

[10] Yang,J. and Shen,H.S., Vibration characteristics and transient response of shear-deformable functionally graded plates in thermal environments. *Journal of Sound and Vibration*, 2002, 255: 579-602.

[11] Matsunaga,H., Free vibration and stability of angle-ply laminated composite and sandwich plates under thermal loading. *Composite Structures*, 2007, 77: 249-262.

[12] Pradeep,V. and Ganesan,N., Buckling and vibration of rectangular composite viscoelastic sandwich plates under thermal loads. *Composite Structures*, 2007, 77: 419-429.

[13] Pradeep,V. and Ganesan,N., Thermal buckling and vibration behavior of multi-layer rectangular viscoelastic sandwich plates. *Journal of Sound and Vibration*, 2008, 310: 169-183.

[14] Jeyaraj,P., Ganesan,N. and Padmanabhan,C., Vibration and acoustic response of a composite plate with inherent material damping in a thermal environment. *Journal of Sound and Vibration*, 2009, 320: 322-338.

[15] Geng,Q. and Li,Y.M., Analysis of dynamic and acoustic radiation characteristics for a flat plate under thermal enveronment. *International Journal of Applied Mechanics*, 2012, 4(3): 1250028.

[16] Yang,X.W., Chen,G. and Li,Y.M., Topology optimization of a bi-material plate with respect to sound radiation in a thermal environment. *International Journal of Aerospace and Lightweight Structures*, 2012, 2: 87-102.

[17] Yang,X.W. and Li,Y.M., Topology optimization to minimize the dynamic compliance of a bi-material plate in a thermal environment. *Struct Multidisc Optim*, 2013, 47: 399-408.

[18] Liu,Y. and Li,Y.M.. Vibration and acoustic response of rectangular sandwich plate under thermal environment. *Shock and Vibration*, 2013, 20: 1011-1030.